Atmos. Meas. Tech. Discuss., 7, 5347–5379, 2014
www.atmos-meas-tech-discuss.net/7/5347/2014/
doi:10.5194/amtd-7-5347-2014
© Author(s) 2014. CC Attribution 3.0 License.

Atmospheric Measurement Techniques Discussions
Open Access

This discussion paper is/has been under review for the journal Atmospheric Measurement Techniques (AMT). Please refer to the corresponding final paper in AMT if available.

Satellite observations of peroxyacetyl nitrate from the Aura Tropospheric Emission Spectrometer

V. H. Payne[1], M. J. Alvarado[2], K. E. Cady-Pereira[2], J. R. Worden[1], S. S. Kulawik[3], and E. V. Fischer[4]

[1]Jet Propulsion Laboratory, California Institute of Technology, Pasadena, California, USA
[2]Atmospheric and Environmental Research, Lexington, Massachusetts, USA
[3]Bay Area Environmental Research Institute, Mountain View, California, USA
[4]Colorado State University, Fort Collins, Colorado, USA

Received: 7 May 2014 – Accepted: 16 May 2014 – Published: 3 June 2014

Correspondence to: V. H. Payne (vivienne.h.payne@jpl.nasa.gov)

Published by Copernicus Publications on behalf of the European Geosciences Union.

Abstract

We present a description of the algorithm used to retrieve peroxyacetyl nitrate (PAN) concentrations from the Aura Tropospheric Emission Spectrometer (TES). We describe the spectral microwindows, error analysis and the utilization of a priori and initial guess information provided by the GEOS-Chem global chemical transport model. The TES PAN retrievals contain up to one degree of freedom for signal. Estimated single-measurement uncertainties are 30 to 50 %. The detection limit for a single TES measurement is dependent on the atmospheric and surface conditions as well as on the instrument noise. For observations where the cloud optical depth is less than 0.5, we find that the TES detection limit for PAN is in the region of 200 to 300 pptv. We show that PAN retrievals over the Northern Hemisphere Pacific in springtime show spatial features that are qualitatively consistent with the expected distribution of PAN in outflow of Asian pollution.

1 Introduction

Peroxyacetyl Nitrate (PAN) is a thermally unstable reservoir for active nitrogen (NO_x) that allows NO_x to be transported over large distances, enabling efficient ozone formation far downwind from the original source (Singh and Hanst, 1981; Hudman et al., 2004; Fischer et al., 2010; Singh, 1987). The dissociative lifetime of PAN is strongly dependent on air mass temperature, being longer than one month at temperatures characteristic of the mid-troposphere, but only of the order of one hour at 20 °C. The stability of PAN at mid-tropospheric temperatures allows the compound to be transported on a hemispheric scale. PAN therefore plays a fundamental role in the long-range transport of NO_x and in the global O_3 budget.

Existing aircraft and surface observations show that PAN is present in the atmosphere at mixing ratios ranging from a few pptv in the remote marine atmosphere to several ppbv in polluted urban environments and biomass burning plumes (e.g. Singh

AMTD
7, 5347–5379, 2014

CC BY

and Salas, 1986; Ridley et al., 1990; Singh et al., 1990, 1998; Fischer et al., 2010). However, aircraft and surface measurements of PAN have primarily been campaign-based and therefore limited in spatial and temporal coverage (Fischer et al., 2014 and references therein). The existing suite of in situ observations provide only snapshots of the global atmospheric PAN distribution. Given the very limited set of long-term measurements, there are gaps in our knowledge of the distribution, seasonal cycle and interannual variability of PAN and the processes driving these features.

Satellite observations provide opportunities to collect information on a global scale, over multi-year timescales. PAN is readily detectable via satellite remote sensing in the thermal infrared region. PAN has previously been retrieved in the upper troposphere and lower stratosphere from limb observations on a global scale from the Envisat Michelson Interferometer for Passive Atmospheric Sounding (MIPAS) (Moore and Remedios, 2010; Wiegele et al., 2012) and from the Canadian Atmospheric Chemistry Experiment Fourier Transform Spectrometer (ACE-FTS) (Tereszchuk et al., 2013). PAN signatures have also been observed in nadir observations of smoke plumes from fires by both the Aura Tropospheric Emission Spectrometer (TES) (Alvarado et al., 2011) and MetOp-A Infrared Atmospheric Sounding Instrument (IASI) (Clarisse et al., 2011), but to our knowledge, PAN has not previously been retrieved in the nadir view on a global scale.

Building on the detection of PAN in TES radiances described by Alvarado et al. (2011), we have developed a PAN retrieval product for TES. Here we describe the algorithm and the product. In Sect. 2, we provide background on the TES instrument, including information on temporal and spatial sampling. In Sect. 3, we describe the TES PAN retrieval and in Sect. 4, show initial results for the northern Pacific in April 2008.

AMTD
7, 5347–5379, 2014

CC BY

2 TES measurements

The Aura TES instrument, a nadir-viewing Fourier transform spectrometer measuring thermal-infrared radiances with extremely high spectral resolution (0.06 cm^{-1}), provides information on a large number of different trace gases, including PAN.

The TES instrument uses a 16 element detector array. The total surface footprint is 8 by 5 km at nadir (0.5 by 5 km footprint for each detector). The nominal mode of the instrument is "global survey" mode, where TES makes periodic measurements every ~ 200 km along the satellite track. Other measurement modes are step-and-stare mode and transect mode. In step and stare mode, nadir measurements are made every 40 km along the track for some specified latitude range. In transect mode, a series of 40 consecutive scans spaced 12 km apart is performed, providing relatively dense coverage over a limited area.

Figure 1 shows a simulated TES spectrum, alongside the the PAN signature (difference between simulations with and without PAN) for a PAN profile with a peak value of 0.4 ppbv. The same magnitude of PAN signal in TES measurements can result from different PAN profiles. In fact, Fig. 1b shows the simulated signal for two example PAN profiles (shown in Fig. 2), for the case where all aspects of the atmospheric and surface state, other than PAN, were kept constant, but the results from the two different profiles are not distinguishable by eye. Figure 1 also shows the optical depth contributions from PAN and other molecules with signatures in this spectral region. It can be seen that there is strong interference in this region from water vapor (H_2O), deuterated water vapor (HDO), ozone (O_3), nitrous oxide (N_2O) and CFC-12. Addtional interfering species in this region (not shown in Fig. 1) include HFC-23, HCFC-141b, CFC-113, HFC-134a, HCFC-22, CFC-114, CFC-115, HFC-152a, and HFC-125. However these molecules have very weak signatures compared to PAN.

AMTD
7, 5347–5379, 2014

CC BY

3 PAN retrievals

3.1 Forward model

The forward model component of the TES operational retrieval is described in detail in Clough et al. (2006). The TES forward model is based on the Line-By-Line Radiative Transfer Model (LBLRTM) (Clough et al., 2005; Alvarado et al., 2012). The required inputs include the temperature profile, profiles for relevant molecular species, cloud and aerosol characteristics, and the parameters necessary to describe the radiative properties of the surface.

The spectroscopic input used here for PAN are the cross section data from the HITRAN 2008 compilation (Rothman et al., 2009), which were in turn taken from the work of Allen et al. (2005a, b).

3.2 Retrieval approach

The TES PAN retrieval uses an optimal estimation approach (Rodgers, 2000; Bowman et al., 2006). Provided that the retrieved state is close to the true state, the retrieved state can be expressed as:

$$\hat{\boldsymbol{x}}_{\mathrm{a}} = \boldsymbol{x}_{\mathrm{a}} + \mathbf{A}(\boldsymbol{x} - \boldsymbol{x}_{\mathrm{a}}) + \mathbf{G}\boldsymbol{n} + \mathbf{G}\mathbf{K}_b(\boldsymbol{b} - \boldsymbol{b}_{\mathrm{a}}), \tag{1}$$

where $\hat{\boldsymbol{x}}_{\mathrm{a}}$, $\boldsymbol{x}_{\mathrm{a}}$, and $\boldsymbol{x}$ are the retrieved, a priori, and the "true" state vectors. The state vectors are expressed as the natural logarithm of volume mixing ratio (VMR) for TES trace gas retrievals. The gain matrix, $\mathbf{G}$, maps from radiance space into profile space. The vector $\boldsymbol{n}$ is the noise on the spectral radiances. The vector $\boldsymbol{b}$ represents the true state for parameters that affect the modeled radiance but are not included in the retrieval state vector (such as calibration, concentrations of interfering gases, etc.). The vector $\boldsymbol{b}_{\mathrm{a}}$ holds the corresponding a priori values. The Jacobian, $\mathbf{K}_b = \partial\mathbf{L}/\partial\boldsymbol{b}$, describes the sensitivity of the forward modeled radiances $\mathbf{L}$ to the vector $\boldsymbol{b}$.

AMTD
7, 5347–5379, 2014

CC BY

The averaging kernel, **A**, describes the sensitivity of the retrieved state to the true state:

$$\mathbf{A} = \frac{\partial \hat{\boldsymbol{x}}}{\partial \boldsymbol{x}} = \left(\mathbf{K}^{\mathrm{T}}\mathbf{S}_{\mathrm{n}}^{-1}\mathbf{K} + \mathbf{S}_{\mathrm{a}}^{-1}\right)^{-1}\mathbf{K}^{\mathrm{T}}\mathbf{S}_{\mathrm{n}}^{-1}\mathbf{K} = \mathbf{GK} \tag{2}$$

Here, **K** is the sensitivity of the forward modeled radiances to the state vector ($\mathbf{K} = \partial\mathbf{L}/\partial\hat{\boldsymbol{x}}$). The noise covariance matrix, $\mathbf{S}_{\mathrm{n}}$, represents the noise in the measured radiances. $\mathbf{S}_{\mathrm{a}}$ is the constraint matrix for the retrieval.

For profile retrievals, the widths of the rows of **A** provide a measure of the vertical resolution of the retrieval. Provided that the retrieval is relatively linear, the sum of each row of **A** indicates the fraction of retrieval information that comes from the measurement as opposed to the a priori at a given altitude (Rodgers, 2000). The trace of the averaging kernel matrix gives the number of degrees of freedom for signal (DOFS), or independent pieces of information, for the retrieval.

The PAN retrievals are carried out after the retrievals of temperature, water vapor, ozone, carbon dioxide, methane, nitrous oxide, deuterated water vapor, cloud optical depth, cloud height, and surface temperature and emissivity. For these quantities, we use the output from the v05 TES Level 2 algorithm as input to the initial step for the PAN retrieval process. (TES Level 2 products are publicly available from the Langley Research Center Atmospheric Science Data Center – see http://asdc.larc.nasa.gov/search/tes/.)

Previous retrieval steps do not utilize the spectral regions immediately adjacent to the PAN feature. We choose to re-fit for surface emissivity using spectral windows located on either side of the PAN absorption feature before attempting the retrieval of PAN itself. This provides a baseline for the additional absorption from PAN. We then assume that the surface emissivity varies linearly across the PAN spectral region. The microwindows used for the emissivity and PAN retrieval steps are shown in Table 1.

As stated above, the retrieval minimizes differences between observed and calculated radiances. The difference between observed and calculated radiances can be

AMTD
7, 5347–5379, 2014

CC BY

expressed in terms of a cost function:

$$\chi^2 = (\boldsymbol{y} - \mathbf{F}(\hat{\boldsymbol{x}}))^{\mathrm{T}} \mathbf{S}_{\mathrm{n}}^{-1} (\boldsymbol{y} - \mathbf{F}(\hat{\boldsymbol{x}})) \quad (3)$$

A χ^2 value equal to 1.0 indicates that the radiances are fit within the expected noise. Since the PAN signal is generally relatively weak compared to the noise on the TES radiances, we find that there are incidences where the residuals at the point of the PAN initial step show features that would overwhelm the PAN signal, making a PAN retrieval unfeasible. (This will be discussed in more detail in Sect. 3.6.) Therefore, we choose not to attempt PAN retrievals for cases where the χ^2 value at the initial PAN step is greater than 3.0. The value of 3.0 was determined empirically.

3.3 A priori constraints

We have chosen to use a monthly-varying prior constraint for the TES PAN retrievals, based on information from state-of-the-science simulations from the GEOS-Chem global chemical transport model. The GEOS-Chem PAN simulations as used here are described in detail in Fischer et al. (2014). The model is broadly consistent with existing surface and aircraft observations, which in themselves do not provide sufficient coverage from which to build a climatology. Existing observations lead us to expect certain features in the global distribution of PAN. Figure 3 shows GEOS-Chem PAN distributions for April, July and September 2008. This figure shows three main features of the global distribution: a springtime surface maximum in PAN in the Northern Hemisphere, a maximum aloft in Northern Hemisphere in summer, and a maxiumum aloft in the Tropical South Atlantic in the austral spring. Starting from a monthly mean GEOS-Chem simulation on a 4° latitude by 5° longitude grid, we created six a priori profiles for each month, using the following approach. First, we categorized all model profiles into tropical regions (18° S to 18° N) and regions outside the tropics, in order to account for the variation in the tropopause with latitude. Profiles were classified as clean if the maximum concentration within the profile was less than 0.3 ppbv, and enhanced otherwise. Enhanced profiles were further classified according to whether the

AMTD
7, 5347–5379, 2014

CC BY

maximum PAN value occurred at a pressure higher than 600 hPa (surface maximum) or at a pressure less than 600 hPa (maximum aloft). The profiles for each of these six categories were averaged. The a priori profiles for the month of July are shown in Fig. 4 as an example. Since little information exists about variations in the global distribution of PAN from one year to the next, we use the same a priori profiles for all years of TES data.

For each model grid box, we assign a category and use the relevant average profile as the retrieval a priori. At the start of the retrieval, the observation co-ordinates and month are used to select the relevant a priori profile. The initial guess for each retrieval is always set to a profile with a uniform value of 0.3 ppbv in the troposphere. (The stratospheric values follow the GEOS-Chem profiles, which drop off rapidly above the tropopause.) The idea is to have a high initial guess value, in order to avoid entering null space on the first step in the retrieval, and to have a uniform tropospheric value in an attempt to avoid forcing the retrieval towards surface-maximum versus maximum-aloft profiles. The a priori profile is therefore different than the initial guess.

Our a priori uncertainties are high, and we might expect to encounter interesting cases (e.g. in plumes) where our truth may be far from the a prior profiles. We have therefore used a relatively relaxed retrieval constraint. The PAN constraint matrix used here is diagonal, with diagonal elements set to $(\ln(3.0))^2$ for all retrieval levels. For nadir retrievals, where vertical information is limited, it is common practice to introduce off-diagonal elements in the constraint matrix in order to avoid spurious oscillations in the retreived profile. Due to the nature of the broad PAN spectral feature, or perhaps to the relatively coarse spectral resolution of the PAN cross-section data used in the forward model, we found that the retrieval did not attempt to obtain better fits by introducing oscillations in the profile, and we did not find it necessary to introduce off-diagonal elements in the constraint matrix.

AMTD
7, 5347–5379, 2014

CC BY

3.4 Retrieval characteristics

The PAN signals in the TES spectra are relatively weak compared to the noise level of the instrument (see Fig. 1). Therefore, the amount of information on PAN that can be retrieved from a single scan is somewhat limited. Figure 5 shows an example TES PAN retrieval for a measurement within a boreal fire plume (as determined by Alvarado et al., 2010, 2011), with associated averaging kernels. In this example, we see peak sensitivity to PAN at 300–400 hPa, with ~ 1.0 degrees of freedom for signal (DOFS) for the retrieval. While the pressure range of the peak sensitivity varies according to atmospheric and surface conditions, and the averaging kernels may peak much lower in the atmosphere for some cases where the peak in PAN concentration is near-surface, we find that the shape of the averaging kernels shown here is representative of the majority of TES PAN retrievals. In general, the number of DOFS is less than 1.0. Therefore, the TES PAN retrievals cannot provide information about the vertical structure of the PAN profile.

3.5 Insight from simulated retrievals

In order to evaluate the performance of the retrieval algorithm, we performed a set of retrievals from simulated radiances for one TES global survey from July 2008 (2786 observations). The "true" PAN profiles for these simulations were from GEOS-Chem simulations for the same month. Other atmospheric and surface parameters (temperature, traces gases, cloud optical depth, cloud top height, surface temperature and surface emissivity) for the simulations were taken from the version 5 TES Level 2 products. Atmospheric and surface state information were used as input to the TES forward model in order to simulate top-of-atmosphere radiances and random noise based on TES instrument noise characteristics was added to the calculated radiances. We also simulated radiances for the same set of profiles, but with zero PAN. We calculated the PAN signal in each case by subtracting the "zero-PAN" spectrum from the "with-PAN" spectrum for each case.

AMTD
7, 5347–5379, 2014

CC BY

We then calculated a signal-to-noise (SNR) value for each case, using the difference between the "with-PAN" ($\boldsymbol{L}_{\mathrm{PAN}}$) and the "zero-PAN" ($\boldsymbol{L}_{\mathrm{NO\_PAN}}$) radiances and the TES noise for the PAN microwindows.

$$\mathrm{SNR} = (\boldsymbol{L}_{\mathrm{PAN}} - \boldsymbol{L}_{\mathrm{NO\_PAN}})^{\mathrm{T}} \mathbf{S}_{\mathrm{n}}^{-1} (\boldsymbol{L}_{\mathrm{PAN}} - \boldsymbol{L}_{\mathrm{NO\_PAN}}) \tag{4}$$

The same GEOS-Chem fields were used here for truth here as were used to generate the prior. Therefore, in this simulation environment, the a priori state vector does (as it should) represent our knowledge of some mean state.

Figure 6a shows a two-dimensional histogram of the SNR against the peak PAN concentration in the true profiles. (No retrieval is involved in the generation of this panel – only profile input and simulated radiances.) 600 of the 2786 cases show SNR > 1.0. Since PAN is a relatively weak signal in TES spectra, we had the expectation that we would only detect PAN in cases with low cloud optical depth (Alvarado et al., 2011). We find from these simulations that with a cloud optical depth threshold of 0.5, we retain 1709 of the original 2786 cases and of those, 538 show SNR > 1.0. This provides a rough indication that TES can likely observe elevated PAN for cases where the cloud optical depth is less than 0.5. This cloud optical depth threshold is approximate. If the PAN VMR were extremely high, a cloud optical depth greater than 0.5 would not necessarily prevent detection of the signal.

From Fig. 6a, we also see that on the lower-PAN edge of the histogram, a SNR value of 1.0 corresponds very roughly to a "maximum PAN" value of 0.2 ppbv. From this, we infer an approximate detection limit of 0.2 ppbv.

We performed PAN retrievals from the "with-PAN" simulated radiances. For this set of retrievals, the surface and atmospheric state were known perfectly. This is significantly less complicated than the situation when performing retrievals from real data, where there is inherent uncertainty associated with the additional surface and atmospheric parameters, even for those that have been retrieved in previous steps of the algorithm. These retrievals from simulations can provide insight into the limitations of the retrieval under idealized conditions.

AMTD
7, 5347–5379, 2014

CC BY

The limit of detection for the TES PAN retrievals is key to the determination of how the product can be used for science. We can think of the limit of detection as the atmospheric PAN concentration needed for the retrieval to return a value that has a significant contribution from the measurement, rather than just the a priori. Figure 6b shows a two-dimensional histogram of the DOFS against the maximum PAN VMR in the true profiles. In general, we see that the DOFS is larger for cases with greater PAN VMRs. We also see that there is a limit of 1 DOFS in the PAN retrieval. If we set a threshold of DOFS > 0.6 in order to distinguish cases where we expect to get a meaningful PAN retrieval, then we would also infer a detection limit in the region of 0.2 ppbv, roughly consistent with SNR = 1.0.

3.6 Error estimates

Sources of uncertainty considered here are listed in Table 2 and discussed in more detail below. These sources of uncertainty can be broadly divided into those that vary randomly from one measurement to the next, those that are systematic (e.g. spectroscopic uncertainty) and those (such as water vapor uncertainty) that are "pseudo-random". Those in the pseudo-random category may have a systematic component, but are still variable from one profile to the next.

In the simulated dataset described in Sect. 3.5, we assume perfect knowledge of everything except the PAN values. This dataset therefore provides the means to evaulate the impact of instrument noise on the retrieval for the case where all other error sources listed in Table 2 are equal to zero. Figure 7 shows the differences between the true and retrieved profiles as function of altitude, as well as the difference between true and retrieved values as a function of the true value. This figure only shows points for which the sum of the row of the averaging kernel is greater than 0.5. We see that for cases with reasonable sensitivity, the RMS differences between the true and retrieved values are generally less than 0.15 ppbv in the lower troposphere and less than 0.1 in the upper troposphere. In general, we also see a positive bias for cases with low true values and a negative bias for cases with higher true values. The reason for this is the

AMTD
7, 5347–5379, 2014

influence of the prior information on the end result. For the low cases, the prior is, on average, higher than the truth and for the high PAN cases, the prior is lower than the truth, introducing some bias. For these retrievals, where the DOFS is always less than 1.0, we must accept some influence of the prior.

There is some uncertainty associated with the absolute radiance calibration of the TES instrument. Previous work (Connor et al., 2011; Shephard et al., 2008a) has also shown some systematic offsets between TES filters, of the order of tenths of Kelvin. However, our retrieval strategy should mitigate the impact of this uncertainty on the PAN retrieval. (We re-retrieve cloud and surface emissivity before the PAN step, in order to set a baseline against which the PAN signal can be assessed.) Similarly, if the surface emissivity and the cloud optical depth can be assumed to vary linearly with wavenumber across the $\sim 40\,\mathrm{cm}^{-1}$ wide PAN spectral region, we can assume that the impact of uncertainties in these quantities are also made small by out choice of retrieval strategy. Connor et al. (2011) showed that the TES radiances exhibit excellent stablility between 2005 and 2009. Subsequent work (T. Connor, personal communication, 2012) indicate that the radiances remain stable between 2010 and 2012. Therefore, drift in the radiance calibration in time should not a concern for use of the TES PAN retrievals for assessing long-term variations such as interannual variability.

Systematic errors in the PAN cross-section data used as input to the forward model would also result in systematic errors in the PAN retrieval. An error in the integrated band intensity of the PAN cross-section would be expected to translate (roughly) into the same percentage error in the retrieved PAN VMR. Here, we used PAN cross sections from the HITRAN 2008 compilation (Rothman et al., 2009), which were in turn taken from the work of Allen et al. (2005a, b). These measurements were made at three temperatures in order to capture the temperature dependence of the cross section, but no measurements were recorded at temperature belwo 250 K. Allen et al. (2005a) cite uncertainties in the integrated band intensity of around 5 % for the band used here, but this does not include the extrapolation error below 250 K. Following the logic of Tereszchuk et al. (2013), we assume a value of $\sim 8\,\%$ for the spectroscopic error.

AMTD
7, 5347–5379, 2014

CC BY

Interfering species (see Fig. 1) are another potential source of unceratinty in the PAN retrievals. For the TES PAN retrievals, H_2O is the dominant interfering species in the spectral range used. H_2O is highly variable in space and time. The impact of H_2O uncertainties is mitigated by our choice of microwindows and by the strategy of retrieving H_2O in a previous step. Validation of previous versions of the TES H_2O product indicate rms agreement of 25–45 % with in-situ validation data (Shepard et al., 2008b). Using the simulated dataset described in Sect. 3.5, we performed an additional set of retrievals where we scaled the H_2O in the initial guess atmospheric state for the PAN retrievals by random scaling factors with a standard deviation of 45 %. We found that the RMS difference in the retrieved PAN between the perturbed H_2O set and the reference dataset was less than 0.1 ppbv, although we do find that there are isolated cases where an underestimate in the H_2O can lead to spurious high retrieved PAN values. For this reason, we require a good quality flag from the TES H_2O retrieval for any given measurement before attempting a PAN retrieval.

We would expect the impact of the other interfering species to be small compared to that of water vapor. Although both O_3 and N_2O have relatively strong features in the spectral windows that we are using, neither of these molecules show a smooth variation that would be confused with a PAN signature. We do require that the O_3 and N_2O retrieved in previous retrieval steps pass basic quality flags before a PAN retrieval is attempted. However, significant errors in these molecules would result in a high initial χ^2 value (Sect. 3.2), which would likely mean that a PAN retrieval would not be attempted in any case. CFC-12 does show a smooth variation in the PAN spectral region. However, we assume that CFC-12 is extremely well-mixed, that the value is well known, and that uncertainties associated with CFC-12 are small compared to other terms. We assume that the error associated with other CFCs and HFCs with spectral features in this region is extremely small compared to the error associated with water vapor.

Uncertainties in the temperature profile are another potential source of uncertainty in the PAN retrievals. Uncertainties in the TES temperature retrievals are of the order

AMTD
7, 5347–5379, 2014

CC BY

of a couple of Kelvin. Here, we assume that the unceratinties associated with the PAN cross sections are significantly larger than the uncertainty associated with the retrieved temperature profile.

4 Example retrieval results: April 2008 over the Pacific

Figure 8 shows a map of TES observations of elevated PAN over Eastern Asia, the Pacific and the Western US for one month (April 2008) in springtime, the season when we expect to see a strong contribution of Asian transport to US air pollution. The figure shows cases where the DOFS for the PAN retrieval is greater than 0.6. This threshold was chosen to be roughly consistent with SNR > 1 in the simulated results shown in Fig. 6. TES detects elevated PAN in a non-negligible number of cases. Note that we do not have sufficient information in the TES spectra to be able to determine the vertical distribution of the PAN in the atmosphere.

It is clear from Fig. 8 that the TES PAN retrievals are highly variable spatially. We might expect that elevated PAN would often be seen in plumes. Validation of the TES PAN product against in-situ data will therefore require good spatial and temporal coincidences between TES and in-situ data, for cases where elevated PAN is observed. Ideally, validation of the TES PAN retrievals would involve aircraft profiles. To date, suitable validation data have not been available. Validation of the TES PAN product against independent observations will be a subject of future work.

We do see cases where the PAN values retrieved by TES are > 2 ppbv. In situ aircraft observations of PAN conducted in spring 2008 conducted as part of the ARCPAC (Aerosol, Radiation and Cloud Processes affecting Arctic Climate) campagin also indicate elevated (1–3 ppbv) abundances of PAN associated with plumes of smoke originating in regions of intense biomass buring in Russia (Roberts et al., 2009). Screening out cases according to the TES H_2O quality flag did remove a handful of high PAN cases, but not all of them. We note that the uncertainties on the TES PAN retrieval are relatively high (30–50 %), but these estimates seem reasonable given the heavy impact

AMTD
7, 5347–5379, 2014

CC BY

of northern Eurasian biomass burning on the atmosphere at this time (Warneke et al., 2009, 2010).

Other aspects of the geographical distribution of elevated PAN values also appear as we might expect, with a higher density of elevated PAN detections and generally higher PAN values over the East Asian source region, and generally lower values and lower density of detections going out over the Pacific. The sporadic nature of extremely elevated PAN in biomass burning smoke is also reflected at high northern latitudes, extending from Russia across the Northern Pacific. To explore this in a more quantitative way, we looked at the proportion of elevated PAN detections relative to the total number of TES observations in four latitude/longitude boxes which separately represent the polluted Asian coast and immediate outflow region, the eastern Pacific and the Arctic (Fig. 9).

In the box over Asia, we see the highest occurence of elevated PAN detections, with elevated PAN detected in 9.5 % of TES observations. The box over Asia also shows a higher occurence of very high PAN values than the Eastern Pacific. We see fewer PAN detections over the Eastern Pacific (4.2 %). We also see a higher incidence of elevated PAN values (6.6 %) in the southern part of the West coast of North America. The retrieved values in this region are generally lower than those observed over Asia, and we speculate that this pattern is driven by North American pollution, where reactive nitrogen pollution advected off the coast and recirculated over the eastern Pacific. The Arctic region has a relatively high density of total TES observations. Although the incidence of elevated PAN values (3.1 %) is not as high as in the other highlighted regions, the Arctic shows the highest incidence of extreme high PAN values (> 1.5 ppbv). We speculate that these high values are associated with springtime fires in northern Eurasia.

AMTD
7, 5347–5379, 2014

CC BY

5 Summary/conclusions

We can detect elevated PAN in TES spectra. We use initial data from April 2008 as an example here. During this month, PAN was detected in ∼ 10 % of TES observations over the Asian pollution source region, and elevated PAN over the North American Arctic associated with wildfires in Russia was also detected. The TES radiance dataset provides global coverage over multi-year timescales, providing opportunities for investigations of tropopspheric PAN on spatial and temporal scales that have not been possible with in-situ measurements.

Results from simulated retrievals suggest that TES can detect PAN in profiles where the maximum value is around 200 pptv, although the presence of elevated PAN values in the atmosphere viewed by TES does not guarantee that TES can detect PAN. The detection of PAN in TES spectra is also subject to the atmospheric and surface conditions.

The uncertainty on TES PAN retrievals is of the order of 30 to 50 %. The error budget is largely dominated by the instrument noise. However, since PAN is highly spatially variable, and TES is not capable of measuring "background" PAN levels, the TES PAN dataset is not suitable for simple spatial averaging. We suggest that the utility of the TES PAN dataset will lie in providing information on the frequency of incidence of elevated PAN on a global scale and on multi-year timescales.

The retrieval approach presented here could potentially be applied to other nadir infrared sounders, such as the Infrared Atmospheric Sounding Instrument (IASI) and the Atmospheric InfraRed Sounding Instrument (AIRS). These instruments have lower spectral resolution than TES, but significantly greater spatial coverage, providing increased probablility of observing high-PAN plumes.

Acknowledgements. This research was carried out at the Jet Propulsion Laboratory, California Institute of Technology, under a contract with the National Aeronautics and Space Administration. Reference herein to any specific commercial product, process or service by trade name,

AMTD
7, 5347–5379, 2014

CC BY

trademark, manufacturer, or otherwise, does not constitute or imply its endorsement by the United States Government or the Jet Propulsion Laboratory, California Institute of Technology.

References

Allen, G., Remedios, J. J., Newnham, D. A., Smith, K. M., and Monks, P. S.: Improved mid-infrared cross-sections for peroxyacetyl nitrate (PAN) vapour, Atmos. Chem. Phys., 5, 47–56, doi:10.5194/acp-5-47-2005, 2005a.

Allen, G., Remedios, J. J., and Smith, K. M.: Low temperature mid-infrared cross-sections for peroxyacetyl nitrate (PAN) vapour, Atmos. Chem. Phys., 5, 3153–3158, doi:10.5194/acp-5-3153-2005, 2005b.

Alvarado, M. J., Logan, J. A., Mao, J., Apel, E., Riemer, D., Blake, D., Cohen, R. C., Min, K.-E., Perring, A. E., Browne, E. C., Wooldridge, P. J., Diskin, G. S., Sachse, G. W., Fuelberg, H., Sessions, W. R., Harrigan, D. L., Huey, G., Liao, J., Case-Hanks, A., Jimenez, J. L., Cubison, M. J., Vay, S. A., Weinheimer, A. J., Knapp, D. J., Montzka, D. D., Flocke, F. M., Pollack, I. B., Wennberg, P. O., Kurten, A., Crounse, J., Clair, J. M. St., Wisthaler, A., Mikoviny, T., Yantosca, R. M., Carouge, C. C., and Le Sager, P.: Nitrogen oxides and PAN in plumes from boreal fires during ARCTAS-B and their impact on ozone: an integrated analysis of aircraft and satellite observations, Atmos. Chem. Phys., 10, 9739–9760, doi:10.5194/acp-10-9739-2010, 2010.

Alvarado, M. J., Cady-Pereira, K. E., Xiao, Y., Millet, D. B., and Payne, V. H.: Emission ratios for ammonia and formic acid and observations of peroxy acetyl nitrate (PAN) and ethylene in biomass burning smoke as seen by the Tropospheric Emission Spectrometer (TES), Atmosphere, 2, 633–654, 2011.

Beer, R., Glavich, T. A., and Rider, D. M.: Tropospheric emission spectrometer for the Earth Observing System's Aura satellite, Appl. Optics, 40, 2356–2367, 2001.

Bowman, K. W., Rodgers, C. D., Sund-Kulawik, S., Worden, J., Sarkissian, E., Osterman, G., Steck, T., Luo, M., Eldering, A., Shephard, M. W., Worden, H., Clough, S. A., Brown, P. D., Rinsland, C. P., Lampel, M., Gunson, M., and Beer, R.: Tropospheric emission spectrometer: retrieval method and error analysis, IEEE T. Geosci. Remote, 44, 1297–1307, doi:10.1109/TGRS.2006.871234, 2006.

AMTD
7, 5347–5379, 2014

Cady-Pereira, K. E., Shephard, M. W., Millet, D. B., Luo, M., Wells, K. C., Xiao, Y., Payne, V. H., and Worden, J.: Methanol from TES global observations: retrieval algorithm and seasonal and spatial variability, Atmos. Chem. Phys., 12, 8189–8203, doi:10.5194/acp-12-8189-2012, 2012.

Clarisse, L., R'Honi, Y., Coheur, P.-F., Hurtmans, D., and Clerbaux, C.: Thermal infrared nadir observations of 24 atmospheric gases, Geophys. Res. Lett., 38, L10802, doi:10.1029/2011GL047271, 2011 .

Clough, S. A., Shephard, M. W., Worden, J., Brown, P. D., Worden, H. M., Luo, M., Rodgers, C. D., Rinsland, C. P., Goldman, A., Brown, L., Kulawik, S. S., Eldering, A., Lampel, M. C., Osterman, G., Beer, R., Bowman, K., Cady-Pereira, K. E., and Mlawer, E. J.: Forward Model and Jacobians for Tropospheric Emission Spectrometer Retrievals, IEEE T. Geosci. Remote, 44, 1308–1323, 2006.

Coheur, P.-F., Clarisse, L., Turquety, S., Hurtmans, D., and Clerbaux, C.: IASI measurements of reactive trace species in biomass burning plumes, Atmos. Chem. Phys., 9, 5655–5667, doi:10.5194/acp-9-5655-2009, 2009.

Connor, T. C., Shephard, M. W., Payne, V. H., Cady-Pereira, K. E., Kulawik, S. S., Luo, M., Osterman, G., and Lampel, M.: Long-term stability of TES satellite radiance measurements, Atmos. Meas. Tech., 4, 1481–1490, doi:10.5194/amt-4-1481-2011, 2011.

Fischer, E. V., Jaffe, D. A., Reidmiller, D. R., and Jaegle, L.: Meteorological controls on observed peroxyacetyl nitrate at Mount Bachelor during the spring of 2008, J. Geophys. Res., 109, D18302, doi:10.1029/2009jd012776, 2010.

Fischer, E. V., Jaffe, D. A., and Weatherhead, E. C.: Free tropospheric peroxyacetyl nitrate (PAN) and ozone at Mount Bachelor: potential causes of variability and timescale for trend detection, Atmos. Chem. Phys., 11, 5641–5654, doi:10.5194/acp-11-5641-2011, 2011.

Fischer, E. V., Jacob, D. J., Yantosca, R. M., Sulprizio, M. P., Millet, D. B., Mao, J., Paulot, F., Singh, H. B., Roiger, A., Ries, L., Talbot, R. W., Dzepina, K., and Pandey Deolal, S.: Atmospheric peroxyacetyl nitrate (PAN): a global budget and source attribution, Atmos. Chem. Phys., 14, 2679–2698, doi:10.5194/acp-14-2679-2014, 2014.

Gaffney, J. S., Fajer, R., and Senum, G. I.: An improved procedure for high purity gaseous peroxyacetyl nitrate production: use of heavy lipid solvents, Atmos. Environ., 18, 215–218, 1984.

Hudman, R. C., Jacob, D. J., Cooper, O. R., Evans, M. J., Heald, C. L., Pek, R. J., Fesenfeld, F., Flocke, F., Holloway, J., Huebler, G., Kita, K., Koike, M., Kondo, Y., Neuman, A., Nowak, J.,

AMTD
7, 5347–5379, 2014

Oltmans, S., Parrish, D., Roberts, J. M., and Ryersonm, T.: Ozone production in transpacific Asian pollution plumes and implications for air quality in California, J. Geophys. Res., 109, DS23S10, doi:10.1029/2004JD004974, 2004.

Jacob, D. J., Logan, J. A., and Murti, P. P.: Effect of rising Asian emissions on surface ozone in the United States, Geophys. Res. Lett., 26, 2175–2178, 1999.

Kotchenruther, R. A., Jaffe, D. A., and Jaegle, L.: Ozone photochemistry and the role of peroxyacetyl nitrate in the springtime northeastern Pacific troposphere: results from the Photochemical Ozone Budget of the Eastern North Pacific (PHOEBEA) campaign, J. Geophys. Res., 106, 28731–28741, 2001a.

Kotchenruther, R. A., Jaffe, D. A., Beine, H. J., Anderson, T., Bottenheim, J. W., Harris, J., Blake, D., and Schmidt, R. W. H.: Observations of ozone and related species in the northeast Pacific during the PHOBEA campaigns: 2. Airborne observations, J. Geophys. Res., 106, 7463–7483, 2001b.

Kulawik, S. S., Worden, J., Eldering, A., Bowman, K., Gunson, M., Osterman, G. B., Zhang, L., Clough, S., Shephard, M. W., and Beer, R.: Implementation of cloud retrievals for Tropospheric Emission Spectrometer (TES) atmospheric retrievals: part 1. Description and characterization of errors on trace gas retrievals, J. Geophys. Res., 111, D24204, doi:10.1029/2005JD006733, 2006.

Moore, D. P. and Remedios, J. J.: Seasonality of Peroxyacetyl nitrate (PAN) in the upper troposphere and lower stratosphere using the MIPAS-E instrument, Atmos. Chem. Phys., 10, 6117–6128, doi:10.5194/acp-10-6117-2010, 2010.

Nowak, J. B., Parrish, D. D., Newman, J. A., Holloway, J. S., Cooper, O. R., Ryerson, T. B., Nicks Jr., D. K., Flocke, F., Roberts, J. M., Atlas, E. L., de Gouw, J. A., Donnely, S. G., Dunlea, E., Hubler, G., Huey, L. G., Schauffler, S. M., Tanner, D. J., Warneke, C., and Fehsenfeld, F. C.: Gas-phase chemical characteristics of Asian emission plumes observed during ITCT 2K2 over the eastern North Pacific Ocean, J. Geophys. Res., 109, D23S19, doi:10.1029/2003JD004488, 2004.

Payne, V. H., Clough, S. A., Shephard, M. W., Nassar, R., and Logan, J. A.: Information-centered representation of retrievals with limited degrees of freedom for signal: application to methane from the Tropospheric Emission Spectrometer, J. Geophys. Res., 114, D10307, doi:10.1029/2008JD010155, 2009.

Ridley, B. A., Shetter, J. D., Gandrud, B. W., Salas, L. J., Singh, H. B., Carroll, M. A., Hübler, G., Albritton, D. L., Hastie, D. R., Schiff, H. I., Mackay, G. I., Karechi, D. R., Davis, D. D., Brad-

AMTD
7, 5347–5379, 2014

CC BY

shaw, J. D., Rodgers, M. O., Sandholm, S. T., Torres, A. L., Conden, E. P., Gregory, G. L., and Beck, S. M.: Ratios of peroxyacetyl nitrate to active nitrogen observed during aircraft flights over the Eastern Pacific Oceans and continental United States, J. Geophys. Res., 95, 10179–10192, 1990.

Roberts, J. M., Flocke, F., Chen, G., De Gouw, J. A., Holloway, J. S., Hubler, G., Neuman, J. A., Nicks Jr., D. K., Nowak, J. B., Parrish, D., Ryerson, T. B., Sueper, D. T., Warnecke, C., and Fehsenfeld, F. C.: Measurement of peroxycarboxylic nitric anhydrides (PANs) during the ITCT 2K2 aircraft intensive experiment, J. Geophys. Res., 109, D23S21, doi:10.1029/2004JD004960, 2004.

Roberts, J. R., Neuman, J., Nowak, J. B., Ryerson, T. B., Peischl, J. W., Holloway, J., Warneke, C., and de Gouw, J. A.: Measurements of Acylperoxynitrates (PANs) in Biomass Burning Plumes over the Arctic in Spring 2008, American Geophysical Union, Fall Meeting 2009, abstract A43A-0231, 2009.

Rodgers, C. D.: Inverse Methods for Atmospheric Sounding: Theory and Practice, World Sci., Hackensack, NJ, 2000.

Rothman, L. S., Gordon, I. E., Barbe, A., Benner, C. D., Bernath, P. F., Birk, M., Boudon, V., Brown, L. R., Campargue, A., Champion, J.-P., Chance, K., Coudert, L. H., Dana, V., Devi, V. M., Fally, S., Flaud, J.-M., Gamache, R. R., Goldman, A., Jaquemart, D., Kleiner, I., Lacome, N., Lafferty, W. J., Mandin, J.-Y., Massie, S. T., Mikhailenko, S. N., Miller, C. E., Moazzen-Ahmadi, N., Naumenko, O. V., Nitikin, A. V., Orpahl, J., Perevalov, V. I., Perrin, A., Predoi-Cross, A., Rinsland, C. P., Rotget, M., Simeckova, M., Smith, M. A. H., Sung, K., Tashkun, S. A., Tennyson, J., Toth, R. A., Vandaele, A. C., and Vaner Auwera, J.: The HITRAN 2008 molecular spectroscopic database, J. Quant. Spectrosc. Ra., 110, 533–572, 2009.

Shephard, M. W., Worden, H. M., Cady-Pereira, K. E., Lampel, M., Luo, M., Bowman, K. W., Sarkissian, E., Beer, R., Rider, D. M., Tobin, D. C., Revercomb, H. E., Fisher, B. M., Tremblay, D., Clough, S. A., Osterman, G. B., and Gunson, M.: Tropospheric Emission Spectrometer nadir spectral radiance comparisons, J. Geophys. Res., 113, D15S05, doi:10.1029/2007JD008856, 2008a.

Shephard, M. W., Herman, R. L., Fisher, B. M., Cady-Pereira, K. E., Clough, S. A., Payne, V. H., Whiteman, D. N., Comer, J. P., Voemel, H., Miloshevich, L. M., Forno, R., Adam, M., Osterman, G. B., Eldering, A., Worden, J. R., Brown, L. B., Worden, H. M., Kulawik, S. S., Rider, D. M., Goldman, A., Beer, R., Bowman, K. W., Rodgers, C. D., Luo, M., Rinsland, C. P.,

AMTD
7, 5347–5379, 2014

Lampel, M., and Gunson, M. R.: Comparisons of Tropospheric Emission Spectrometer nadir water vapor retrievals with in situ measurements, J. Geophys. Res., 113, D15S24, doi:10.1029/2007JD008822, 2008b.

Singh, H. B.: Reactive nitrogen in the tropospher: chemistry and transport of NO_x and PAN, Environ. Sci. Technol., 21, 320–327, doi:10.1021/es00158a001, 1987.

Singh, H. B. and Hanst, P. L., Peroxyacetyl nitrate (PAN) in the unpolluted atmosphere: an important reservoir for nitrogen oxides, Geophys. Res. Lett., 8, 941–944, doi:10.1029/GL008i008p00941, 1981.

Singh, H. B. and Salas, L. J.: Global distribution of peroxyacetyl nitrate, Nature, 321, 588–591, 1986.

Singh, H. B., Condon, E., Vedder, J., O'Hara, D., Ridley, B. A., Gandrud, B. W., Shetter, J. D., Salas, L. J., Huebert, B. J., Hübler, G., Carroll, M. A., Albritton, D. L., Davis, D. D., Bradshaw, J. D., Sandholm, S. T., Rodgers, M. O., Beck, S. M., Gregory, G. L., and LeBel, P. J.: Peroxyacetyl nitrate measurements during CITE 2: atmospheric distribution and precursor relationships, J. Geophys. Res., 95, 10163–10178, 1990.

Singh, H. B., Viezee, W., Chen, Y., Thakur, A. N., Kondo, Y., Talbot, R. W., Gregory, G. L., Sachse, G. W., Blake, D. R., Bradshaw, J. D., Wang, L., and Jacob, D. J.: Latitudinal distribution of reactive nitrogen in the free troposphere over the Pacific Ocean in late winter/early spring, J. Geophys. Res., 103, 28237–28246, 1998.

Singh, H. B., Brune, W. H., Crawford, J. H., Flocke, F., and Jacob, D. J.: Chemistry and transport of pollution over the Gulf of Mexico and the Pacific: spring 2006 INTEX-B campaign overview and first results, Atmos. Chem. Phys., 9, 2301–2318, doi:10.5194/acp-9-2301-2009, 2009.

Tereszchuk, K. A., Moore, D. P., Harrison, J. J., Boone, C. D., Park, M., Remedios, J. J., Randel, W. J., and Bernath, P. F.: Observations of peroxyacetyl nitrate (PAN) in the upper troposphere by the Atmospheric Chemistry Experiment-Fourier Transform Spectrometer (ACE-FTS), Atmos. Chem. Phys., 13, 5601–5613, doi:10.5194/acp-13-5601-2013, 2013.

Tsalkani, N. and Toupance, G.: Infrared absorptivities and integrated band intensities for gaseous peroxyacetyl nitrate (PAN), Atmos. Environ., 23, 1849–1854, 1989.

Warneke, C., Bahreini, R., Brioude, J., Brock, C. A., de Gouw, J. A., Fahey, D. W., Froyd, K. D., Holloway, J. S., Middlebrook, A., Miller, L., Montzka, S., Murphy, D. M., Peischl, J., Ryerson, T. B., Schwarz, J. P., Spackman, J. R., and Veres, P.: Biomass burning in Siberia and Kazakhstan as an important source for haze over the Alaskan Arctic in April 2008, Geophys. Res. Lett., 36, L02813, doi:10.1029/2008gl036194, 2009.

AMTD
7, 5347–5379, 2014

CC BY

Warneke, C., Froyd, K. D., Brioude, J., Bahreini, R., Brock, C. A., Cozic, J., de Gouw, J. A., Fahey, D. W., Ferrare, R., Holloway, J. S., Middlebrook, A. M., Miller, L., Montzka, S., Schwarz, J. P., Sodemann, H., Spackman, J. R., and Stohl, A.: An important contribution to springtime Arctic aerosol from biomass burning in Russia, Geophys. Res. Lett., 37, L01801, doi:10.1029/2009gl041816, 2010.

Wiegele, A., Glatthor, N., Höpfner, M., Grabowski, U., Kellmann, S., Linden, A., Stiller, G., and von Clarmann, T.: Global distributions of C_2H_6, C_2H_2, HCN, and PAN retrieved from MIPAS reduced spectral resolution measurements, Atmos. Meas. Tech., 5, 723–734, doi:10.5194/amt-5-723-2012, 2012.

Wolfe, G. M., Thornton, J. A., McNeill, V. F., Jaffe, D. A., Reidmiller, D., Chand, D., Smith, J., Swartzendruber, P., Flocke, F., and Zheng, W.: Influence of trans-Pacific pollution transport on acyl peroxy nitrate abundances and speciation at Mount Bachelor Observatory during INTEX-B, Atmos. Chem. Phys., 7, 5309–5325, doi:10.5194/acp-7-5309-2007, 2007.

Zhang, L., Jacob, D. J., Boersma, K. F., Jaffe, D. A., Olson, J. R., Bowman, K. W., Worden, J. R., Thompson, A. M., Avery, M. A., Cohen, R. C., Dibb, J. E., Flock, F. M., Fuelberg, H. E., Huey, L. G., McMillan, W. W., Singh, H. B., and Weinheimer, A. J.: Transpacific transport of ozone pollution and the effect of recent Asian emission increases on air quality in North America: an integrated analysis using satellite, aircraft, ozonesonde, and surface observations, Atmos. Chem. Phys., 8, 6117–6136, doi:10.5194/acp-8-6117-2008, 2008.

AMTD
7, 5347–5379, 2014

Table 1. Microwindows used in the TES PAN retrieval (and preceding emissivity retrieval step).

Target of retrieval	Wavenumber ranges [cm^{-1}]
Surface emissivity	1142.98–1145.98, 1178.98–1180.00
PAN	1154.02–1160.02, 1161.52–1163.02, 1168.00–1169.62

AMTD
7, 5347–5379, 2014

CC BY

Table 2. Sources of uncertainty in TES PAN retrievals.

Uncertainty	Nature of uncertainty	Estimated magnitude for a profile with 0.5 ppbv PAN in the mid-troposphere
Instrument noise	Random	30 %
Bias from a priori	Systematic	Depends on a priori
Absolute instrument calibration	Systematic	Assumed negligible
Spectroscopic uncertainty	Systematic	8 %
H_2O	Pseudo-random	20 %
Other interfering species	Systematic or pseudo random	< 10 %

AMTD
7, 5347–5379, 2014

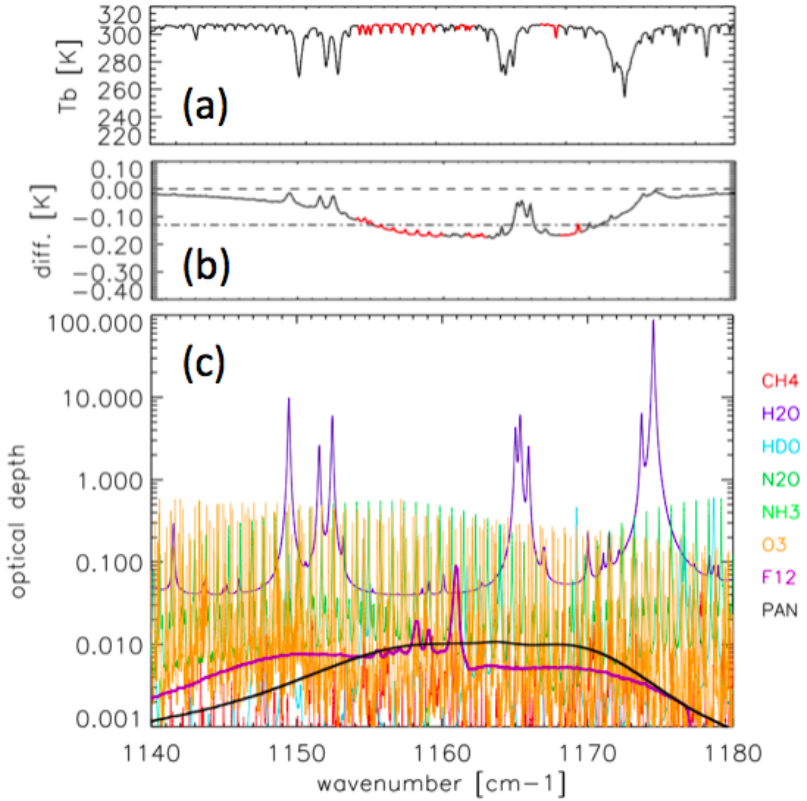

Figure 1. (a) Simulated TES spectrum in the PAN spectral region. Red regions show the spectral regions utilized in the TES PAN retrievals. **(b)** Brightness temperature difference for simulations with and without PAN, for the two PAN profiles shown in Fig. 2. (The signal for these two profiles cannot be distinguished by eye.) Dotted line shows the TES noise for a single observation. **(c)** Optical depth contributions for the dominant interfering species in this spectral region. Species other than PAN are for a US standard atmosphere.

AMTD
7, 5347–5379, 2014

CC BY

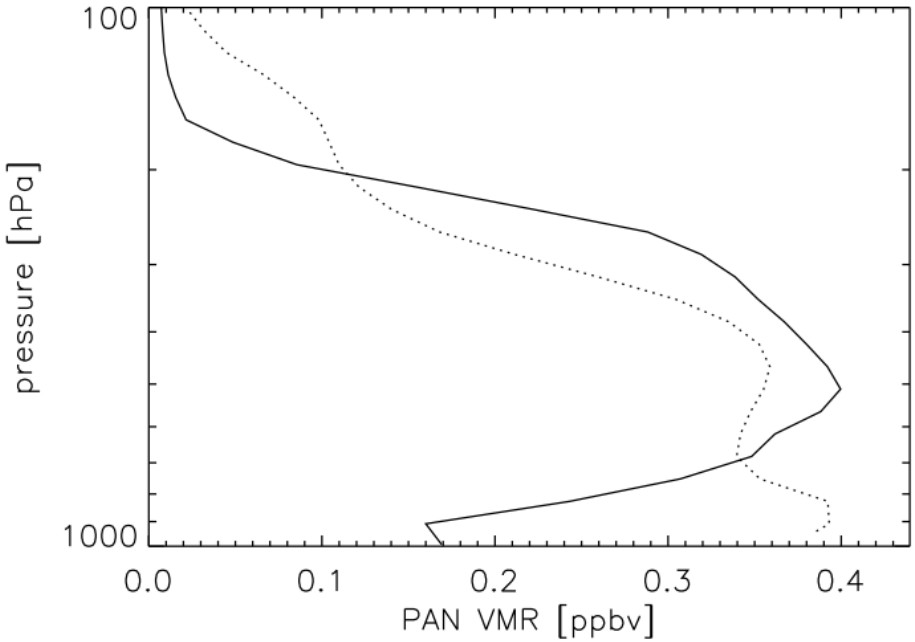

Figure 2. Example of two GEOS-Chem PAN profiles that result in effectively the same signal in TES spectra.

AMTD
7, 5347–5379, 2014

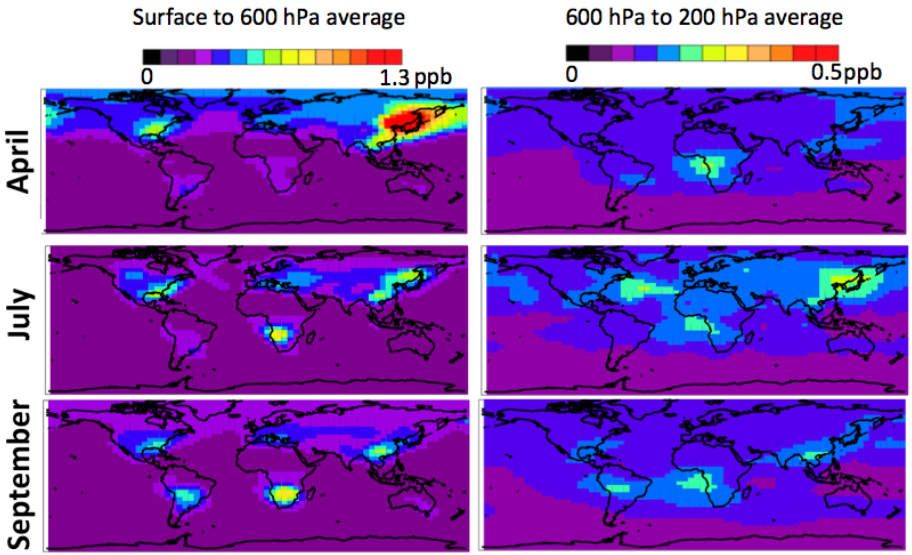

Figure 3. PAN fields from GEOS-Chem. Panels on left show average PAN VMR between 600 hPa and surface for April (top), July (middle) and September (bottom) 2008. Panels on right show averaged VMR between 600 and 200 hPa.

AMTD
7, 5347–5379, 2014

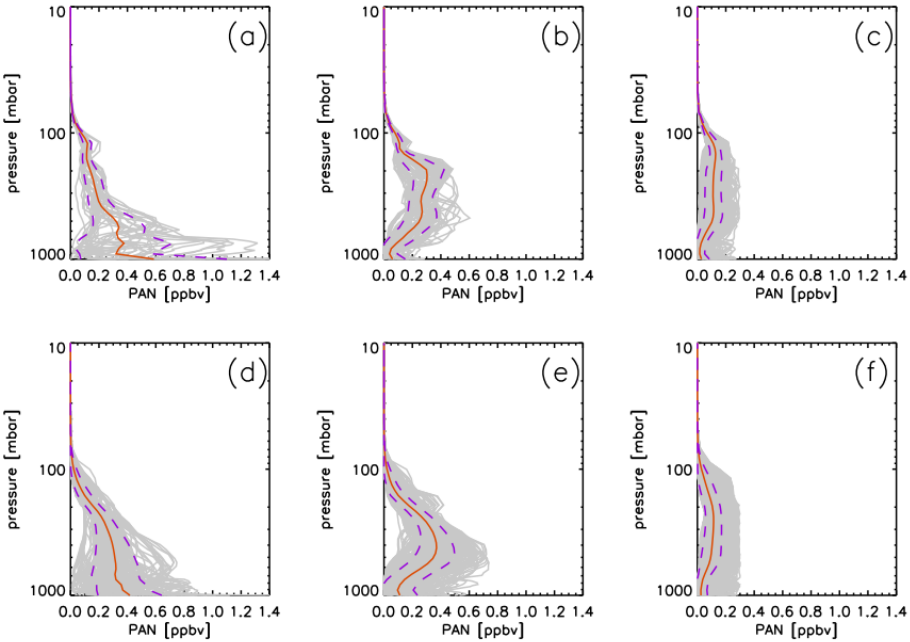

Figure 4. PAN profiles simulated by GEOS-Chem over the whole globe for July 2008, binned by type (in gray): **(a)** tropical profiles with a surface maximum, **(b)** tropical profiles with a maximum aloft, **(c)** tropical profiles with peak value < 0.3 ppbv, **(d)** outside tropics, surface maximum, **(e)** outside tropics, maximum aloft, **(f)** outside tropics, peak value < 0.3 ppbv. The mean profiles for each category (shown in red) are used as a priori profiles in the TES PAN retrieval. Standard deviations about the mean (shown as purple dashed lines) are shown for information, but are not used in the construction of the retrieval constraints.

AMTD
7, 5347–5379, 2014

CC BY

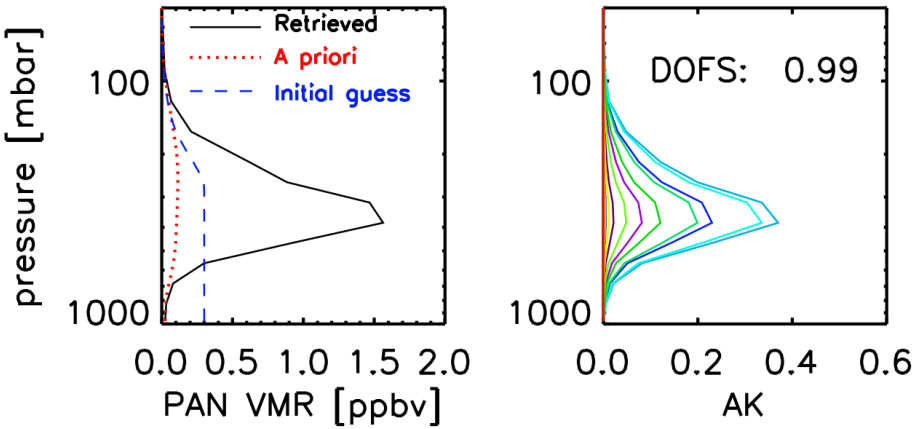

Figure 5. Left: example TES PAN retrieval for a measurement within a boreal fire plume. Right: averaging kernels for this example.

AMTD
7, 5347–5379, 2014

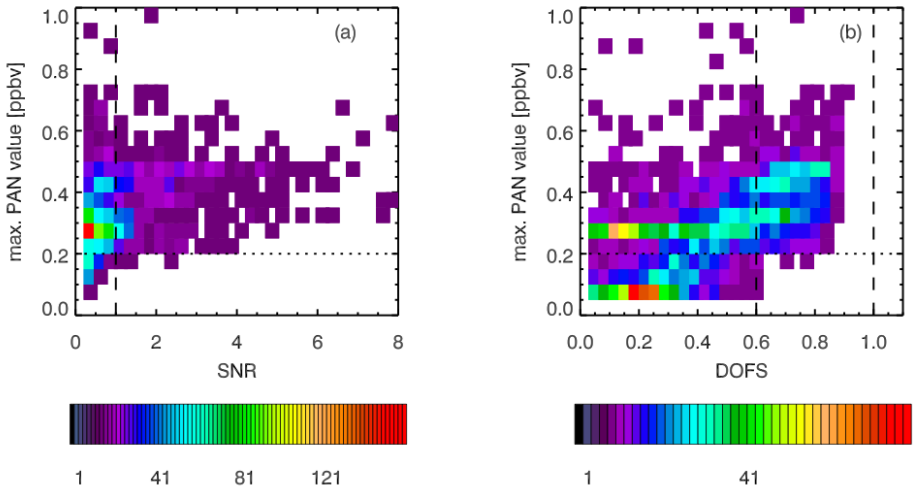

Figure 6. (a) Two-dimensional histogram of signal to noise (SNR) against peak PAN VMR. **(b)** Two-dimensional histogram of DOFS against peak PAN VMR. Color bars show the number of points that fall in each histogram bin.

AMTD
7, 5347–5379, 2014

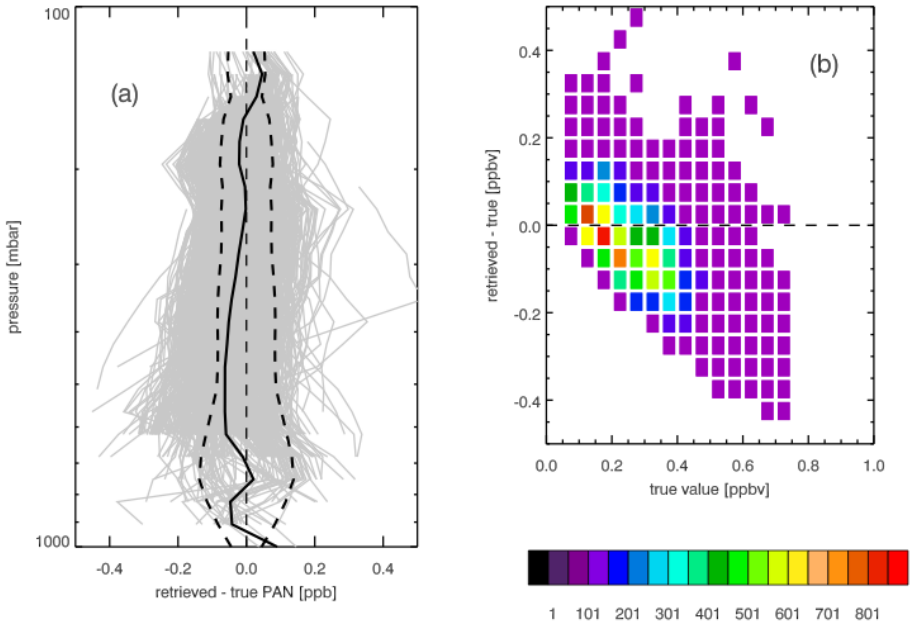

Figure 7. (a) Differences between retrieved and true PAN profiles, for the simulated dataset. **(b)** Two-dimensional histogram of differences between the retrieved and true PAN values as a function of the true values. Only points where the sum of the row of the averaging kernel is greater than 0.5 are shown. Color bar for **(b)** shows the number of points in each histogram bin.

AMTD
7, 5347–5379, 2014

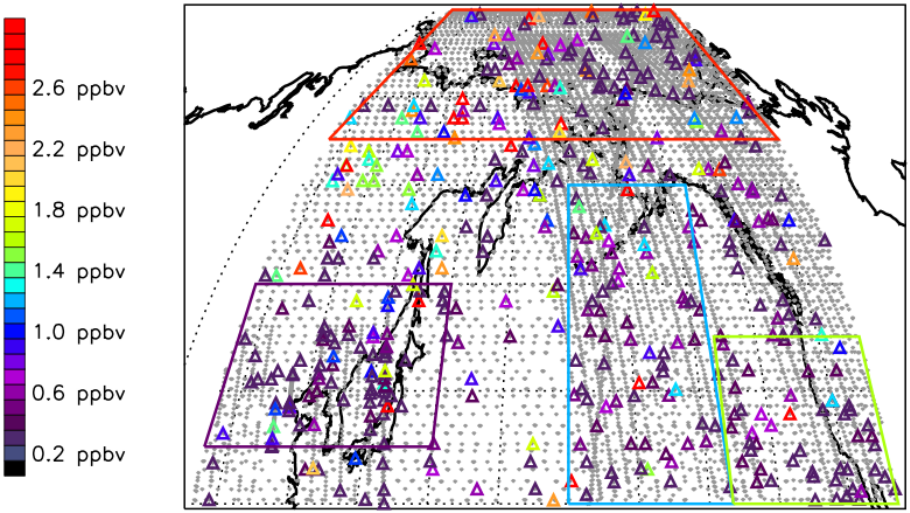

Figure 8. Gray points show all TES observations over the northern Pacific and surrounding land masses for April 2008. Colored triangles show points where elevated PAN was detected in the TES spectra with some confidence (DOFS > 0.6). The VMR values represent the average over all points in the profile where the sum of the row of the averaging kernel is greater than 0.5. Colored latitude/longitude boxes highlight the regions associated with the histograms in Fig. 9.

AMTD
7, 5347–5379, 2014

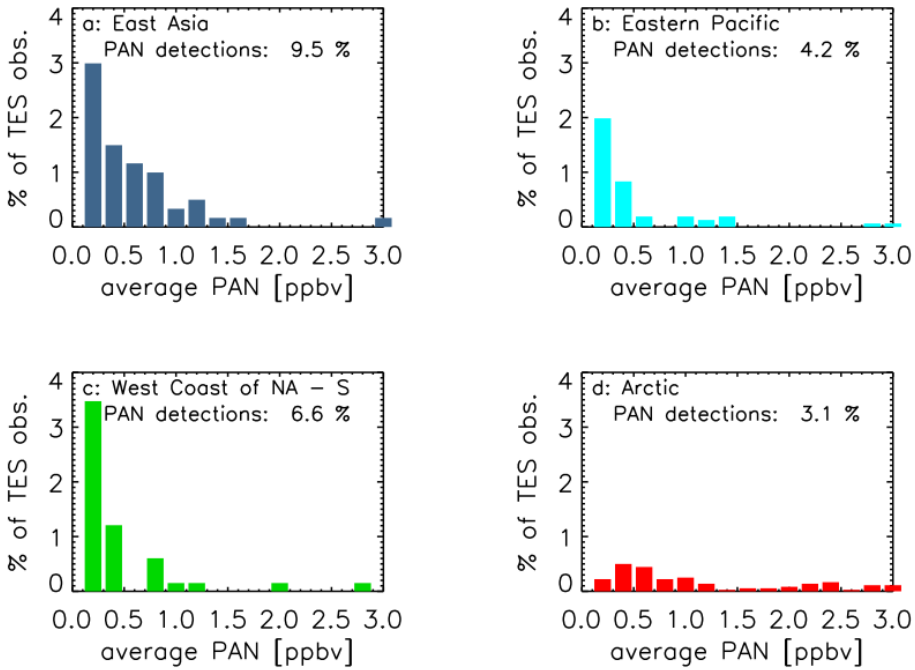

Figure 9. Incidences of elevated PAN as observed by TES during April 2008 in the latitude/longitude boxes shown in Fig. 8. VMR values represent the average for points in the profile where the sum of the row of the averaging kernel is greater than 0.5.

AMTD
7, 5347–5379, 2014

CC BY